

# Nuclear Magnetic Resonance as a probe of nanometre-size orbital textures in magnetic transition metal oxides

G. Papavassiliou<sup>1</sup>, M. Pissas<sup>1</sup>, M. Beles<sup>2</sup>, M. Fardis<sup>1</sup>, D. Stamopoulos<sup>1</sup>, A. Kontos<sup>1</sup>, M. Hennion<sup>3</sup>, J. Dolinsek<sup>4</sup>, J. P. Ansermet<sup>5,2</sup>, and C. Dimitropoulos<sup>1,2</sup>

<sup>1</sup>Institute of Materials Science, NCSR, Demokritos, 153 10 Aghia Paraskevi, Athens, Greece

<sup>2</sup>Dept. of Physics, Ames Laboratory, Iowa State University, Ames, Iowa 50011

<sup>3</sup>Laboratoire Leon Brillouin, CEA-CNRS, CE-Saclay, 91191 Gif sur Yvette, France

<sup>4</sup>Josef Stefan Institute, Jamova 39, 61111 Ljubljana, Slovenia

<sup>5</sup>Dept. of Physics, University of Illinois, Urbana, Illinois 1801, USA

(dated: April 14, 2024)

The study of strong electron correlations in transition metal oxides with modern microscopy and diffraction techniques unveiled a fascinating world of nanosize textures in the spin, charge, and crystal structure. Examples range from high  $T_c$  superconducting cuprates and nickelates, to hole doped manganites and cobaltites. However, in many cases the appearance of these textures is accompanied with "glassiness" and multiscale/multiphase effects, which complicate significantly their experimental verification. Here, we demonstrate how nuclear magnetic resonance may be uniquely used to probe nanosize orbital textures in magnetic transition metal oxides. As a convincing example we show for the first time the detection of nanoscale orbital phase separation in the ground state of the ferromagnetic insulator  $\text{La}_{0.875}\text{Sr}_{0.125}\text{MnO}_3$ .

PACS numbers: 75.47.Lx, 76.60.-k, 75.30.Et, 73.22.-f

It is widely accepted by now that orbital ordering is a key property, which controls the electronic behaviour of many transition metal oxides [1, 2, 3, 4]. A seminal case is  $\text{LaMnO}_3$  [5, 6], where at temperatures lower than  $T_{\text{JT}} \approx 780\text{K}$ , cooperative Jahn-Teller (JT) distortions force an antiferro-orbital ordering within the ab plane. This orbital arrangement defines the magnetic order of the ground state via the Goodenough-Kanamori-Anderson rules: Spins are coupled ferromagnetically in the ab planes and antiferromagnetically along the c axis, giving rise to the so called A-type antiferromagnetic (AFM) spin ordering. By substituting La with a divalent cation such as Sr, the JT-active  $\text{Mn}^{3+}$  sites are replaced by Jahn-Teller-inactive  $\text{Mn}^{4+}$  sites, thus introducing into the system holes and energizing ferromagnetic (FM) coupling through the double exchange mechanism [7]. New orbital structures are thus established [8, 9, 10, 11].

From the crystallographic perspective, by increasing doping  $x$  the ground state of the  $\text{La}_{1-x}\text{Sr}_x\text{MnO}_3$  (LSMO) changes from the JT distorted orthorhombic  $O'$  phase (canted AFM insulating), in the low doping regime, to the almost cubic-orthorhombic  $O$  phase (FM and metallic) at  $x = 0.20$ , as shown in the lower panel of Figure 1 [12, 13]. Around  $x = 0.125$  the system exhibits a peculiar FM and charge ordered (CO) ground state with nominally "pseudocubic" crystal structure, which is known in the literature as  $O''$  structure. The phase transition route for the  $x = 0.125$  system as a function of temperature is clearly seen in the SQUID and ac-susceptibility measurements, in the upper panel of Figure 1. Three successive phase transitions are observed at temperatures  $T_{\text{JT}} \approx 283\text{K}$ ,  $T_c \approx 183\text{K}$ , and  $T_{\text{CO}} \approx 150\text{K}$ . The former transition (inset in the upper panel of Figure 1) is related with the passage from the high temperature pseu-

dobic  $O$  phase to the JT-distorted  $O'$  phase [10, 14], while the latter marks the transition to the CO and orbitally reordered  $[10]O''$  phase. Besides, the large difference in the zero-field cooling and field cooling routes in the SQUID magnetization measurements is indicative of glassy freezing and metastability effects. Similar freezing effects have been observed in other Ca-doped manganites [15, 16], as well as in high  $T_c$  superconducting cuprates [17]. Most spectacularly, upon x-ray irradiation the charge ordered phase is partially destroyed below  $40\text{K}$ , being restored only after heating above  $T_{\text{CO}}$  and subsequent cooling [18, 19]. The thermal history dependence of this effect and the observed photoinduced structural relaxation [18], indicates that the  $O''$  phase is extremely sensitive to the JT-induced strain fields, while showing a tendency to nanoscale phase separation [18]. Here, by using the NMR radiofrequency (rf) enhancement method [20], we uncover an important –but invisible until now – orbital phase separation in the ground state of  $x = 0.125$  LSMO. Specifically, we show that below  $30\text{K}$  the FM and charge ordered  $O''$  matrix phase becomes unstable against the formation of FM nanodomains with the  $O$ -type orbital and crystal structure.

To show this intriguing orbital nanotexturing,  $^{139}\text{La}$  NMR rf enhancement measurements in zero external magnetic field were performed on three high quality LSMO single crystals, with doping  $x = 0.075; 0.125$ , and  $0.20$ . NMR in magnetic materials differs from conventional NMR techniques in several aspects [20]. The most obvious difference is the presence of a spontaneous magnetic hyperfine field,  $B_{\text{hf}} = \frac{1}{h} A \hbar S_i$  at the position of the resonating nuclei, where  $A$  and  $\hbar S_i$  are the hyperfine coupling constant and the average electronic spin,

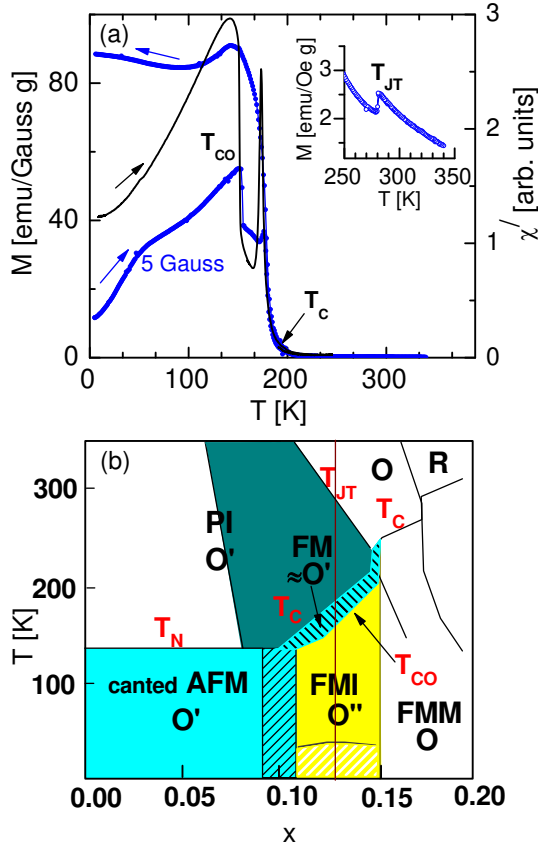


FIG. 1: The magnetic and structural phase transitions of  $\text{La}_{1-x}\text{Sr}_x\text{MnO}_3$  in the  $T$ - $x$  region of interest. (a) SQUID magnetization measurements at 5 Gauss (blue curve), and ac-susceptibility measurements (black curve), performed on a high quality  $x = 0.125$  single crystal. (b) The  $T$ - $x$  phase diagram, in the doping range  $0 \leq x \leq 0.2$ , as reconstructed from refs. [12, 13], by including magnetization and NMR data from the present work. The yellow-white hatched low temperature region around  $x = 0.125$  is characterized by nucleation of FM  $\text{O}'$ -type nanodomains into the  $\text{O}'$  matrix. (FM I = FM insulating, FM M = FM metallic).

respectively. According to this formula, the hyperfine field  $B_{\text{hf}}$  (La) at the position of the spinless ( $S = 0$ ) La sites in LSMO compounds is expected to reflect the average spin state of the surrounding Mn octant, as well as possible deformations of the Mn-O-Mn bonding, which alter the hyperfine coupling constant  $A$  [15, 21]. A less apparent but very important difference is the existence of the rf enhancement [20, 21]. In FM materials, very strong NMR signals are produced at extremely low rf irradiation fields  $B_1$ , due to coupling of the rf field with the magnetic moments of the electrons. Specifically, the applied transverse rf field  $B_1$  produces an internal field  $B_1 = (1 + N)$ , where  $N$  is the demagnetizing factor, and the magnetic susceptibility. The magnetization then rotates through an angle  $B_1 = (1 + N)B_A$ , where  $B_A$  is the magnetic anisotropy field. The rotation of the magnetization at the radiofrequency thus produces an effective

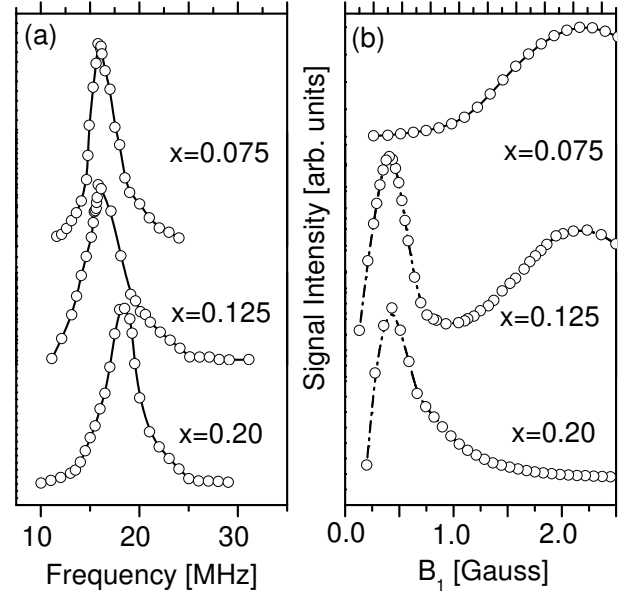


FIG. 2: (a) Zero field  $^{139}\text{La}$  NMR spectra of LSMO for  $x = 0.075; 0.125$ , and  $0.20$ , at  $5\text{K}$ . (b) The  $^{139}\text{La}$  NMR signal intensity  $I$  vs. the rf field  $B_1$  for  $x = 0.075; 0.125$ , and  $0.20$ .

tive rf field  $B_{1,\text{eff}}$  sufficiently stronger than the applied  $B_1$  by the factor  $n = [B_{\text{hf}}/(1 + N)B_A]$ . We notice that the rf enhancement factor  $n$  would decrease in an external magnetic field, while at low fields both domain rotations and domain-wall displacements are expected to contribute to the transverse magnetization. However, in strongly inhomogeneous systems like CMR manganites, rf enhancement experiments reflect directly the local  $B_A$  in the various magnetic subphases [21].

Figure 2 shows zero field  $^{139}\text{La}$  NMR line shape measurements and rf enhancement plots at  $5\text{K}$  for the three systems under investigation. The line shapes were acquired by applying a two pulse spin-echo technique with pulse widths  $t_{p1} = t_{p2} = 0.6$  sec, after recording the integrated spin-echo signal intensity  $I$  at successive irradiation frequencies. The rf enhancement experiments were performed by recording  $I$  as a function of the applied rf field  $B_1$ . The obtained  $I$  vs.  $B_1$  curves follow an asymmetric bell-shaped law with maximum at  $n B_1 = 2\pi/\gamma$ , where  $\gamma$  is the rf pulse duration, the nuclear gyromagnetic ratio, and  $n$  the rf enhancement factor [22]. According to the measurements no major changes are observed in the line shapes of the investigated samples, either with doping  $x$  (Figure 2a), or with temperature variation (not shown in the plot). Specifically, by increasing  $x$  the NMR spectra shift only slightly in frequency from  $16\text{MHz}$  for  $x = 0.075$  to  $18\text{MHz}$  for  $x = 0.20$ , indicating a nearly FM environment for the resonating nuclei in all three cases. The observation of FM NMR signals for  $x = 0.075$  is in agreement with "in field"  $^{139}\text{La}$  NMR line shape measurements for LSMO, with  $0 \leq x \leq 0.15$ , which show a very sharp changeover from the AFM to

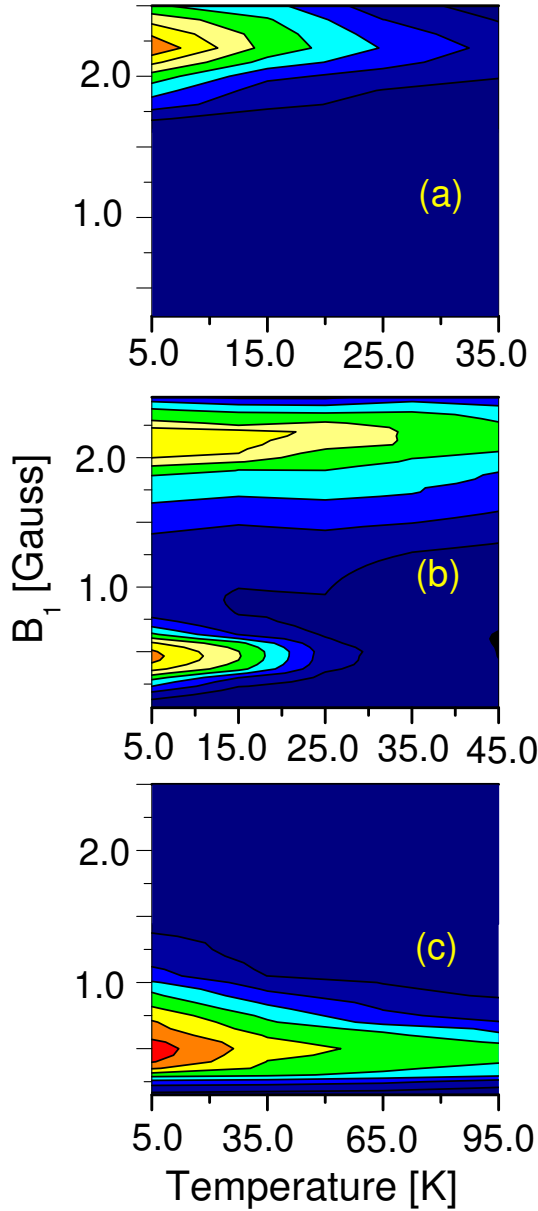


FIG. 3:  $^{139}\text{La}$  NMR rf enhancement experiments for  $\text{La}_{1-x}\text{Sr}_x\text{MnO}_3$  with (a)  $x = 0.075$ , (b)  $x = 0.125$ , and (c)  $x = 0.20$ . The contour plots show the NMR signal intensity  $I$  as a function of  $B_1$  and  $T$ . There is a significant difference in the rf enhancement by varying doping. The plot in the middle shows clearly that the ground state of the LSMO  $x = 0.125$  is a mixture of two phases differing in their magnetocrystalline anisotropy.

the FM phase at  $x = 0.05$  [23]. Besides, neutron scattering experiments have shown the presence of a single "FM modulated" canted AFM state for  $0.06 \leq x \leq 0.1$  [24, 25], comprised of FM platelets, a few unit cells large on the ab plane, which are exchange coupled through the canted AFM matrix.

Contrary to the line shape measurements, a significant difference as a function of doping and temperature

is observed in the rf-enhancement experiments. According to Figure 2b the value  $B_{1\text{max}}$ , where the maximum NMR signal is obtained, is shifted from 2.2 Gauss for  $x = 0.075$  (with the JT-distorted  $O'$  type crystal structure) to 0.5 Gauss for  $x = 0.20$  (with the orthorhombic, and nearly isotropic  $O$  crystal structure). Most important, for  $x = 0.125$  the rf enhancement curve at 5K is a superposition of the corresponding curves for the  $x = 0.075$  and  $0.20$  systems, indicating the spontaneous splitting of the system in two phases with indistinguishable spin-structures, but different magnetocrystalline anisotropy. The evolution of this exciting phase separation by varying temperature can be nicely followed in the contour plots of Figure 3. For  $T > 30\text{K}$  a single phase is observed in Figure 3b, which can be attributed to the  $O''$  structure with antiferro-orbital ordering [26], while at  $T \leq 30\text{K}$  a second phase component appears, resembling the  $O$  structure of the  $x = 0.20$  system. We stress that synchrotron X-rays diffraction experiments observe only  $O''$ -type nanodomains with average size  $\sim 30 - 35\text{ nm}$  [18]. Evidently, the  $O$ -type phase component is confined into smaller "invisible" regions, which increase in size and become detectable only after strong illumination with X-rays [18]. The nucleation of such  $O$ -type islands explains the fast decrease of the antiferro-orbital ordering, observed with resonant X-ray scattering experiments in the low temperature regime of the  $O''$  phase [26]. It is also worth to notice the similarity in the contour plots of the  $O'$  and  $O''$  phases. A possible explanation is that at low doping, such as  $x = 0.075$ , the observed NMR signals are solely produced in FM platelets [24, 25] which are precursors of the  $O''$  phase. However, the size ( $\sim 2\text{ nm}$ ) and the strong coupling of such platelets with the canted AFM matrix state [24, 25], suggests that their anisotropy should be rather determined by the anisotropy of the  $O'$  matrix state. It is thus possible that despite the different orbital hybridization of the  $O'$  and  $O''$  phases, the similarity in their orbital ordering (i.e. antiferro-orbital ordering for both phases [26]) gives rise to comparable  $B_A$  values.

Further information about this orbital phase separation, has been obtained by performing  $^{139}\text{La}$  NMR spin-spin relaxation time ( $T_2$ ) measurements on both phase components.  $T_2$ s were measured with the two pulse spin-echo technique, as previously described, by varying the time interval between the two pulses and recording the decay of the spin-echo signal intensity. The experimental data in Figure 4 show that the appearance of the  $O$  phase component is accompanied with a slope change in the  $T_2$  vs.  $T$  curve of the  $O''$  phase component. Most important, below 30K the  $T_2$  curves for both phase components exhibit the same slope, which is indicative of a similar evolution in their spin dynamics by cooling. Hence, the picture that emerges from Figures 3 and 4 is that the  $O''$  phase is metastable, whereas below 30K droplets of the  $O$  phase at nanometer-scale start to nucleate. A possi-

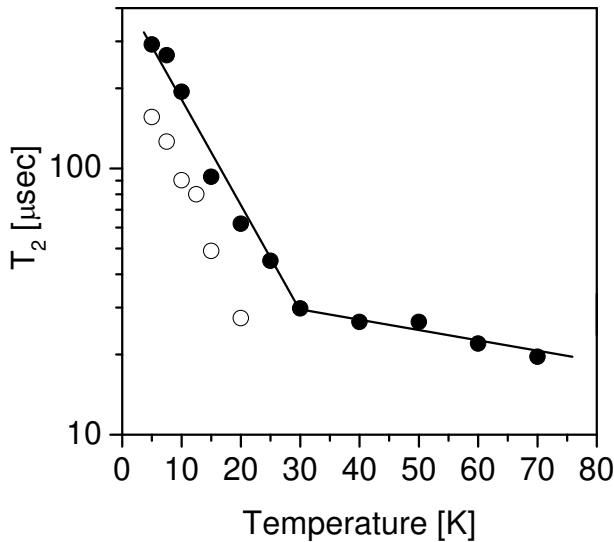


FIG. 4:  $^{139}\text{La}$  NMR spin-spin relaxation time  $T_2$  of  $\text{La}_{0.875}\text{Sr}_{0.125}\text{MnO}_3$  as a function of temperature. Measurements were performed at two different rf fields, i.e. at  $B_1 = 0.5$  Gauss (open circles) and 2.2 Gauss (filled circles), which correspond to signals from the O' and O'' structures, respectively. It is observed that the appearance of O'-type domains is accompanied with a slope change in the  $T_2$  of the signal from the O'' domains.

ble explanation for this behaviour is that strain fields, characterizing the JT-distorted O' phase, are decreasing gradually in the O'' phase, giving rise to undistorted FM metallic islands below a certain transition temperature. A new region, is thus defined in the  $T$  vs  $x$  phase diagram, which is shown as yellow-white hatched region in Figure 1.

In summary, the direct relation between  $B_A$  and the NMR rf enhancement in low doped LSMO, allowed us to unveil an unexpected orbital nanophase separation in the ground state of LSMO,  $x = 0.125$ . This kind of phase separation appears to underlie to the photoinduced phase segregation in LSMO [18], as well as in other CMR manganites [27]. In general, the method we have employed here is applicable in many other magnetic transition metal oxides, where orbital rearrangements are not reflected on the spin structure, but give appreciable dif-

ferences in the local magnetic anisotropy.

<sup>2</sup>Institut de Physique Experimentale, EPFL-PH-Ecublens, 1015-Lausanne, Switzerland

- [1] Y. Tokura and N. Nagaosa, *Science* 288, 462 (2000).
- [2] E. Saitoh, et al, *Nature* 410 180 (2001).
- [3] E. Dagotto, T. Hotta, A. Moreo, *Phys. Rep.* 344, 1 (2001).
- [4] T. Hotta, E. Dagotto, *Phys. Rev. Lett.* 92, 227201 (2004).
- [5] J. Rodriguez-Carvajal, et al, *Phys. Rev. B* 57, R3189 (1998).
- [6] Y. Murakami, et al, *Phys. Rev. Lett.* 81, 582 (1998).
- [7] P.G. de Gennes, *Phys. Rev.* 118, 141 (1960).
- [8] Y. Yamada, et al, *Phys. Rev. Lett.* 77, 904 (1996).
- [9] J. Deisenhofer, et al, *Phys. Rev. B* 68, 214427 (2003).
- [10] J. Geck, et al, *Phys. Rev. B* 69, 104413 (2004).
- [11] T. Mizokawa, D. I. Khomskii, and G. A. Sawatzky, *Phys. Rev. B* 61, R3776 (2000).
- [12] M. Paraskevopoulos, et al, *J. Phys.: Condens. Matter* 12, 3993 (2000).
- [13] G.-L. Liu, J.-S. Zhou, and J.B. Goodenough, *Phys. Rev. B* 64, 144414 (2001).
- [14] S. Uhlenbruck, et al, *Phys. Rev. Lett.* 82, 185 (1999).
- [15] G. Papavassiliou, M. Belesi, M. Fardis and C. Dimitropoulos, *Phys. Rev. Lett.* 87, 177204 (2001).
- [16] V. Markovich, et al, *Phys. Rev. B* 70, 064414 (2004).
- [17] M. H. Julien, et al, *Phys. Rev. B* 63, 144508 (2001).
- [18] V. Kiryukhin, Y. J. Wang, F. C. Chou, M. A. Kastner, R. J. Birgeneau, *Phys. Rev. B* 59, R6581 (1999).
- [19] D. Casa, et al, *Phys. Rev. B* 64, 100404(R) (2001).
- [20] A. C. Gossard and A. M. J. Portis, *Phys. Rev. Lett.* 3, 164 (1959); P. Panissod, C. Meny, *Appl. Magn. Reson.* 19, 447 (2000).
- [21] G. Papavassiliou, et al, *Phys. Rev. Lett.* 91, 147205 (2003).
- [22] G. Papavassiliou et al, *Phys. Rev. B* 55, 15000 (1997).
- [23] K. Kumagai, et al, *Phys. Rev. B* 59, 97 (1999).
- [24] M. Hennen, et al, *Phys. Rev. B* 61, 9513 (2000).
- [25] P. Kober-Lehouelleur, et al, *Phys. Rev. B* 70, 144409 (2004).
- [26] Y. Endoh, et al, *Phys. Rev. Lett.* 82, 4328 (1999).
- [27] K. Miyano, T. Tanaka, Y. Tomioka, and Y. Tokura, *Phys. Rev. Lett.* 78, 4257 (1997).